International Journal of Radiation Oncology biology • physics

www.redjournal.org

Physics Contribution

Toward Personalized Dosimetry with ^{32}P Microparticle Therapy for Advanced Pancreatic Cancer

Yaser Hadi Gholami, MMedPhys,* Nicole Wilson, BSc,† David James, MSc,† and Zdenka Kuncic, PhD*

**Institute of Medical Physics, School of Physics, The University of Sydney, Sydney, New South Wales, Australia; and †OncoSil Medical, Sydney, New South Wales, Australia*

Received Mar 7, 2017, and in revised form Jul 16, 2017. Accepted for publication Jul 24, 2017.

Summary

A Monte Carlo particle simulation platform was developed to model the dosimetry of ^{32}P microparticle internal radionuclide treatment for advanced pancreatic cancer. Patient-specific dosimetry simulations based on data from previous ^{32}P microparticle clinical studies demonstrated the importance of considering non-uniform dose distributions as well as relative dynamic changes in tumor volume and dose rate during treatment. These results will be valuable in designing future personalized treatment strategies.

Purpose: To develop a Monte Carlo model for patient-specific dosimetry of ^{32}P microparticle localized internal radionuclide therapy for advanced pancreatic cancer.

Methods and Materials: Spherical tumor geometries and a pancreatic phantom were modeled, as well as different 3-dimensional non-uniform clinical pancreatic geometries based on patient-specific ultrasound images. The dosimetry simulations modeled the dose distribution due to the energy spectrum of emitted beta particles.

Results: The average dose for small (3-cm diameter) and large (6-cm diameter) spherical tumors was 111 Gy (for 7.6 MBq administered activity) and 128 Gy (for 58 MBq), respectively. For the clinical 3-dimensional geometries, on the basis of patient data, the mean doses delivered to the tumor were calculated to be in the range 102 to 113 Gy, with negligible dose to the pancreas for the smallest tumor volumes. The calculated dose distributions are highly non-uniform. For the largest tumor studied, the pancreas received approximately 6% of the tumor dose (5.7 Gy). Importantly, we found that because the smallest tumor studied exhibited the most dynamic changes in volume in response to the treatment, the dose to tumor and pancreas is significantly underestimated if a static tumor volume is assumed.

Conclusions: These results demonstrate the dosimetry of ^{32}P microparticle localized internal radionuclide therapy for pancreatic cancer and the possibility of developing personalized treatment strategies. The results also highlight the importance of considering the effects of non-uniform dose distributions and dynamic change of tumor mass during treatment on the dosimetry of the tumor and critical organs.

Reprint requests to: Zdenka Kuncic, PhD, School of Physics, The University of Sydney, A28, Sydney, New South Wales 2006, Australia. Tel: (+61) 2-9351-3162; E-mail: zdenka.kuncic@sydney.edu.au

Conflict of interest: Y.H.G. receives salary support from OncoSil Medical. N.W. and D.J. are employed by OncoSil Medical.

Supplementary material for this article can be found at www.redjournal.org.

Acknowledgment—The authors thank the reviewers, whose comments and suggestions helped to improve this article.

Int J Radiation Oncol Biol Phys, Vol. 99, No. 4, pp. 1029–1038, 2017
0360-3016/$ - see front matter
http://dx.doi.org/10.1016/j.ijrobp.2017.07.031

Introduction

Internal radionuclide therapy (IRT) is well established in the field of nuclear medicine for treating different types of cancer (1-3). Phosphorus-32 microparticle therapy is an active implantable (radiologic) medical device intended for use in IRT, whereby cancer is treated by the insertion of radioactive implants directly into the cancerous tissue. It consists of silicon microparticles containing the radioactive phosphorous isotope ^{32}P, which is a pure beta emitter. Phosphorus-32 is one of the most promising radionuclides for localized IRT (LIRT) owing to its ability to localize energy deposition (short-range beta particles) and its long exposure time (98% of the radiation is delivered within 81 days, or approximately 6 half-lives). Additionally, it has been shown that ^{32}P is the most effective therapeutic radionuclide in heterogeneous radioactivity distribution cases when the effective half-life is dominated by the radionuclide physical half-life (4).

Internal radionuclide therapy/LIRT needs to be reliably assessed with personalized (patient-specific) dosimetry calculations to accurately evaluate the efficacy and safety of the therapeutic radionuclide in both clinical and research settings. Although existing standard dosimetry software (eg, OLINDA/EXM) can perform dose calculations for an individual patient's critical organs, it has 2 major shortcomings. First, the software assumes a uniform activity distribution in the source organ for calculating the mean absorbed dose to a target organ. Second, for tumor dosimetry, it does not consider the effect of the dynamic change of the tumor mass or volume and dose rate variation. A previous study (5) showed that for tumors with a short shrinkage half-life (shorter than the radionuclide half-life), the dose correction factor could be as high as 10. These major shortcomings might have led to inaccurate predictions of deterministic biological effects, including tumor response and normal tissue toxicity, attributable to the spatially non-uniform dose in the target and temporally changing dose rates (4-6). Unfortunately there is a lack of experimental and theoretical dosimetry studies on dynamic tumor masses. More generally, there are limited dosimetry studies of IRT/LIRT for pancreatic cancer. The dosimetry of internally distributed radioactivity can, however, be calculated with high accuracy by utilizing Monte Carlo particle simulations (6). Hence, this study aims to develop a Monte Carlo model for patient-specific dosimetry of ^{32}P microparticle LIRT for pancreatic cancer, including the effects of dynamic tumor mass on the dosimetry of the tumor and surrounding pancreas.

Methods and Materials

Monte Carlo simulation

All simulations were performed using GATE7.1 software (7), based on the Geant4 10.1 P01 Monte Carlo toolkit (8), which includes databases for commonly used radionuclides. Phosphorus-32 is a pure beta-emitting radioisotope with a physical half-life of 14.27 days. The mean and maximum energy of the emitted betas is 0.695 MeV and 1.711 MeV, respectively, corresponding to an average and maximum range of 2.8 mm and 8.2 mm in water (7-9). The Geant4 beta particle energy spectrum was imported into GAT, and unless otherwise stated all the simulations were performed using this spectrum.

The stochastic processes of beta emission, hit distribution, associated energy, and dose deposition were simulated using Monte Carlo radiation transport within GATE. The low-energy electromagnetic physics package (10) of Geant4, which describes electron, photon, and light ion interactions over an energy range of 250 eV to 1 GeV, was used for all simulations.

Geometric model of tumor and pancreas

Tumors were initially modeled as spheres with a diameter of either 3 cm (V = 14.1 cm^3) or 6 cm (V = 113.1 cm^3), corresponding to the lower and upper limits of the range of sizes encountered clinically. Each spherical tumor was uniformly filled with water and placed in a cubic water phantom with a side length of 1 m. A source volume ($V_s = 0.08_{tumor}$) was placed at the center of each tumor. Additional simulations were performed with 2 and 3 source volumes (to mimic a multiple-injection scenario) for 3-cm and 6-cm diameter tumors, respectively. The initial specific activity for the 2 and 3 volume sources was divided equally between each volume. Additional simulations were performed for an ellipsoid tumor inside a pancreas phantom (Figs. 1a and 1b). The pancreas phantom was modeled as a half-ellipsoid with a section removed, and an ellipsoid tumor shape with volume of 14.1 cm^3 was placed at the center of the pancreatic head. This model is based on the mathematical human phantom model developed by Cristy and Eckerman (11) for an average adult pancreas size, defined by:

$$\left(\frac{x-x_0}{a}\right)^2+\left(\frac{y}{b}\right)^2+\left(\frac{z-z_0}{c}\right)^2\le 1 \qquad (1)$$

where $a \approx 15$ cm, $b \approx 3$ cm, $c \approx 1$ cm.

$$x > x_0, \text{ and } z \ge z_0$$

Two spherical sources were positioned along the y direction inside the tumor (Fig. 1) for each simulation. Then the average dose to the tumor and pancreas was calculated.

Clinical tumor geometries

Three different non-uniform tumor models with 9 different volumes were modeled on the basis of 2-dimensional (2D) ultrasound images and measured tumor volumes from clinical study patients (Fig. 2). In this clinical study a total of 17 patients with advanced pancreatic cancer were treated with ^{32}P microparticles. All the modeled tumor

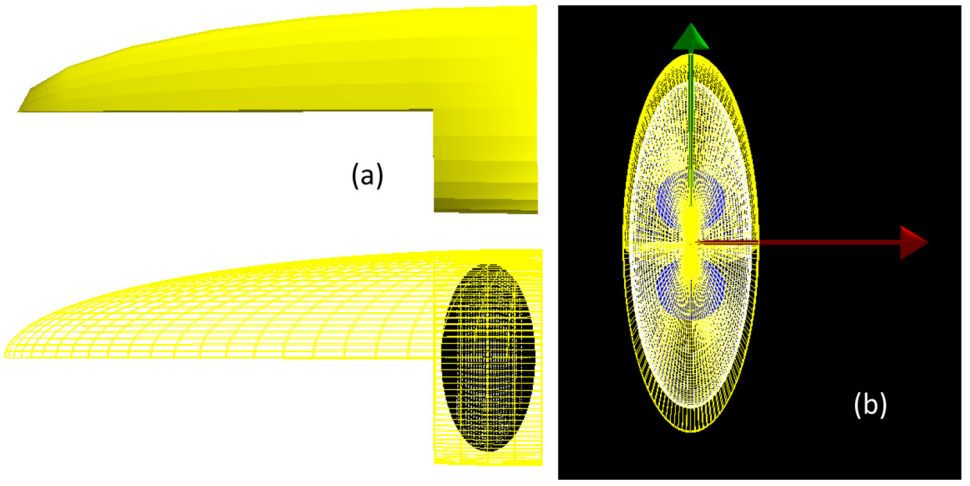

Fig. 1. Geometry setup in the GATE simulation. (a) The pancreas phantom with an ellipsoid tumor at the center of the pancreatic head; (b) ellipsoid tumor in the pancreatic head with boundary closer to the tumor. Two spherical sources (blue spheres) are placed along the *y* direction. The source-target geometry is visualized from the *z* axis view. (A color version of this figure is available at www.redjournal.org.)

volumes were based on data from 3 patients with ultrasound images and 3 other patients whose measured tumor volumes best represented the observed range of small, medium, and large volumes. Because the ultrasound images were 2D, the 3-dimensional (3D) volume of each tumor was modeled for a possible large, medium, and small tumor size (Fig. 2). For each tumor volume size, a number of square and rectangular voxels were used to construct a 3D volume with geometric features similar to the 2D ultrasound images. Voxels were scaled in 3D to obtain initial tumor volumes that matched the clinically measured values, 111, 29.2, and 8.9 cm^3 (see movie provided in Supplementary Materials; available online at www.redjournal.org).

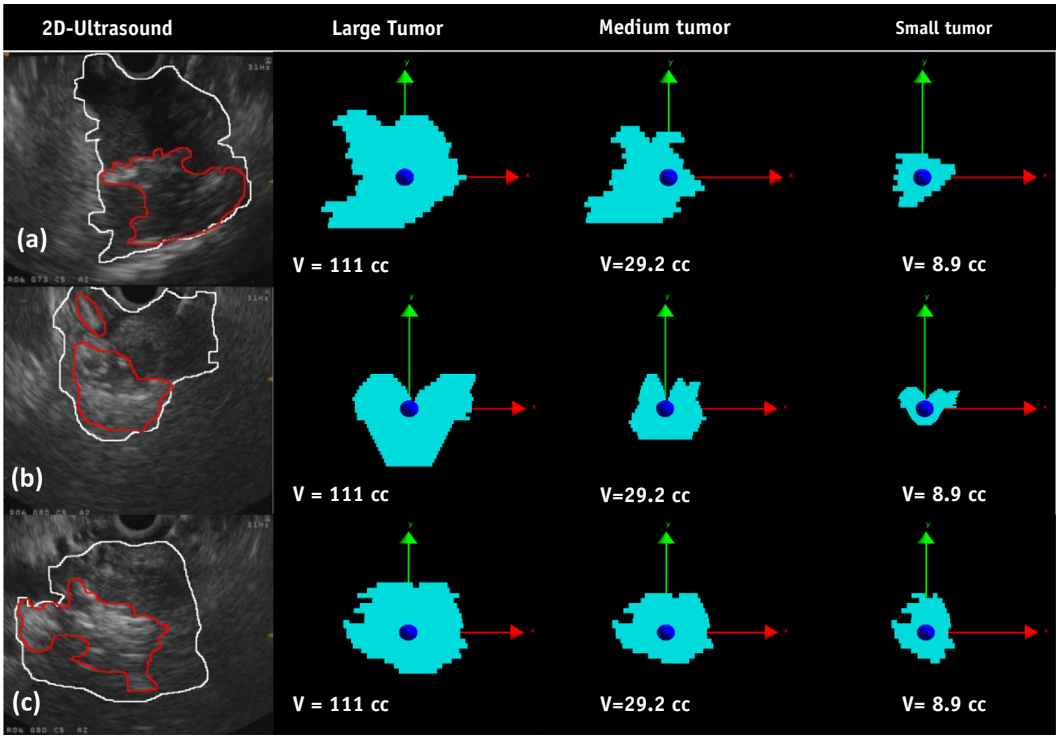

Fig. 2. Geometry of 9 irregularly shaped 3-dimensional tumor models based on clinical 2-dimensional ultrasound images (a-c). White and red margins delineate the tumor and ^{32}P activity distribution, respectively. (A color version of this figure is available at www.redjournal.org.)

Single or multiple ellipsoid sources were modeled in each tumor volume to simulate the spatial activity distribution in the 2D ultrasound images. For all the models the ellipsoid source was positioned in a way that the boundary would be close to or align with the tumor edge. These source-target geometries are intended to represent the worst case scenario that could occur in a clinical setting.

Total number of beta particles and average absorbed dose

The total number of betas emitted in each tumor volume was calculated from the total activity administered clinically. For a typical treatment the prescribed activity concentration is 8% of the tumor volume multiplied by 6.6 MBq/mL. All simulations were performed assuming that 100% of activity remained within the initial volume. The total number of nuclear disintegrations can be estimated using the cumulated activity equation (12):

$$\tilde{A} = \int_0^\infty A_0 e^{-\lambda t} dt = \frac{A_0}{\lambda} = 1.44 \times A_0 t_{1/2} \qquad (2)$$

where $\lambda = -\frac{\ln(2)}{t_{1/2}}$.

For all the simulations a total of 10^{10} beta particles with energies randomly sampled from the ^{32}P spectrum were emitted from the source volume in random directions (Fig. 3a-e). For the spherical tumor models, simulations were also performed using the average beta particle energy, 659 keV, for comparison against the full spectrum. Results were normalized to the total number of beta particles

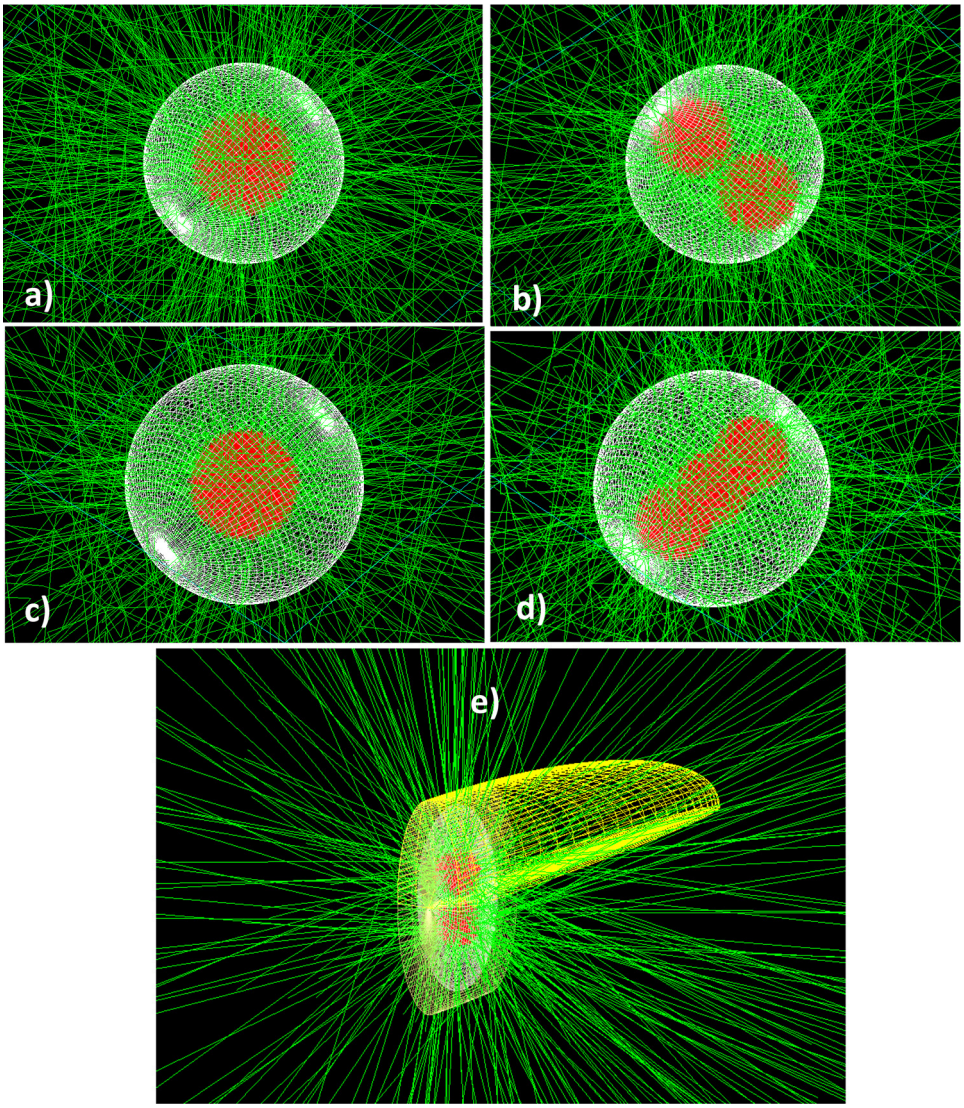

Fig. 3. Source-target geometry. (a, b) Single and double spherical sources at the center of a 3-cm tumor; (c, d) single and triple spherical sources at the center of a 6-cm tumor; (e) pancreas phantom with ellipsoid tumor at the center of the pancreatic head. Red and green tracks represent emitted beta particles and scattered photon trajectories, respectively. (A color version of this figure is available at www.redjournal.org.)

corresponding to each delivered activity. All the phantoms (spherical, pancreatic, and clinical) were voxelized, and parameters such as dose and deposited energy were stored into this 3D matrix according to the spatial position of the hit for each given volume. The average doses were calculated using Equation 3:

$$\tilde{D} = \frac{1}{N}\sum_{i=1}^{n} d_i \qquad (3)$$

where N is the number of voxels and d_i is the computed dose in each voxel. The total number of voxels (with side length of ≈20 μm) for the 3-cm and 6-cm spherical tumor volumes are ≈1.19×10^6 and ≈4.71×10^6, respectively. Additionally, 2D histograms of the dose distribution for different tumor volumes and the pancreas were calculated.

Dynamic tumor volume variation

The dosimetry of a dynamically changing tumor volume was investigated, and the corresponding variations in dose rate and average dose to both tumor and the volume outside the tumor were calculated as follows. The GATE dose results for the small, medium, and large non-uniform clinical tumors (Fig. 2) and pancreas were imported into MATLAB (MathWorks, Natick, MA). The dose in each voxel for both tumor and pancreatic volumes was calculated as a function of the total activity, $\tilde{A}(t)$, to obtain the dose rate as a function of treatment time (total 24 weeks). The total tumor volume variation was modeled according to measurements taken during the clinical study at time points of 0, 8, 16, and 24 weeks from the time of implant. The dose rate as well as the average dose was then calculated for each tumor volume and the pancreas using a polynomial fit to the measured data points. The temporal evolution of the tumor volume was automatically calculated by MATLAB for 1-minute time frames from this continuous polynomial curve. Voxels were adjusted (scaled or removed) to update the 3D dose calculations for each time frame. The activity volume (voxels containing activity) was assumed to remain static throughout, because the ^{32}P microparticles are delivered in a viscous suspension, with limited diffusion.

Results

Dose distribution in spherical and pancreatic tumor models

Figure 4a-d shows 2D dose distributions within the spherical tumor model calculated by integrating the corresponding 3D dose distribution along the z axis. The mean dose to the tumor volume $\tilde{D}_{TV}$ is indicated in each case. These results demonstrate the high degree of dose localization confined to ≈8 mm from the source point and also show that when approximating the beta energy spectrum with the mean energy, $\tilde{D}_{TV}$ is underestimated, by ≈6% for the 3-cm single-source case (Figs. 4a and 4b). The standard deviation (SD_{TV}) values of the dose distributions for the spherical tumor model also demonstrate the high degree of non-uniformity in dose coverage. For the single-source case shown in Figure 4b, for example, the maximum dose is ≈748 Gy, which is ≈3.3 SD above the mean, whereas the minimum dose is ≈0.1 Gy. These coldest voxels represent ≈3% of the total spherical tumor volume. The median dose is ≈10 Gy, which is considerably less than the mean (≈111 Gy) and thus demonstrates that the mean dose is a poor indicator of the dose received by the majority of voxels. The uniform dose coverage is further quantified from the fraction of tumor volume that receives less than 10% and 25% of mean dose, which was calculated to be $V_{\leq 11\ Gy} \approx 49\%$ and $V_{\leq 27.8\ Gy} \approx 63\%$, respectively.

Figure 4e-g shows 2D dose distributions within the pancreas phantom model containing an ellipsoid tumor calculated from the corresponding 3D dose distributions integrated along the z axis. A double ^{32}P source with the full beta energy spectrum was used. Figs. 4h and 4i show the corresponding cumulative dose-volume histograms (CDVHs), compared with those assuming a uniform distribution of dose to the tumor at the mean value, ≈109 Gy. The median dose is 15 Gy and the coldest voxels receive 0.15 Gy, which again demonstrates strong non-uniformity. Similarly, the maximum dose to the tumor is ≈526 Gy (Fig. 4h), which is ≈2.7 SD above the mean. Moreover, ≈46% and ≈59% of total tumor volume receive less than ≈11 Gy (10% of the mean dose) and ≈27 Gy (25% of the mean dose), respectively. These simulations predict that for a prescribed mean dose of $\tilde{D}_{TV} = 109$ Gy delivered to the tumor, the pancreas receives only ≈0.6% on average (ie, ≈0.6 Gy mean dose). The peak dose received by the pancreas is ≈3.5 Gy (Fig. 4i), and the minimum voxel dose is zero.

Dose distribution in clinical tumor geometries

Figure 5 shows the dose distributions of all 9 irregularly shaped clinical tumors with varying volumes, calculated from 2D ultrasound images from 3 individual patients. The red regions indicate the highest dose deposition, whereas the purple regions represent dose deposited by scattered electrons, a small number of bremsstrahlung photons, and a small percentage of emitted energetic beta particles. Corresponding CDVHs for the tumor volume are presented in Supplementary Materials (available online at www.redjournal.org) and demonstrate strong non-uniformity in dose distribution. The tumor volumes receive inadequate dose coverage in some regions, suggesting that multiple sources of ^{32}P may be necessary to achieve clinically significant outcomes. Dose to the pancreas varies from negligible levels to up to 5.7 Gy.

Dosimetry of dynamic tumors

Figure 6 shows the changes in dose rate due to decreasing activity and varying tumor volume for the large, medium,

and small tumors over 24 weeks. The varying tumor volumes were measured for each of the 3 patients, after delivery of ^{32}P microparticles, at 8, 16, and 24 weeks. In all cases, the dose rate dropped to a negligible level in the 16- to 24-week period of the treatment. The large tumor received 58 MBq of ^{32}P microparticle activity. After the first 8 weeks of treatment, the tumor volume decreased from 111 cm^3 to 93.6 cm^3, and by 16 weeks it decreased to 44.7 cm^3. However, the tumor volume increased slightly to 55.4 cm^3 in the third 8-week period. The medium tumor received 15 MBq of ^{32}P microparticle activity, and the volume decreased monotonically from 29.2 cm^3 to 18.4 cm^3 after the first 8 weeks and then to 16.6 cm^3 and 12.8 cm^3 after the second and third 8-week periods, respectively. In the case of the small tumor 5 MBq of ^{32}P microparticle activity was administered, and the tumor volume exhibited a more dynamic response to the treatment compared with the medium and large volumes. The small tumor initially decreased in the first 8 weeks of treatment, from 8.9 cm^3 to 6.3 cm^3, but then increased in size dramatically to 11.7 cm^3 after the second 8 weeks and then decreased again to 6.1 cm^3 after the third 8 weeks.

The results in Figure 6 clearly demonstrate the importance of considering the relative changes in dose rate and tumor volume over treatment time. The dynamic changes in

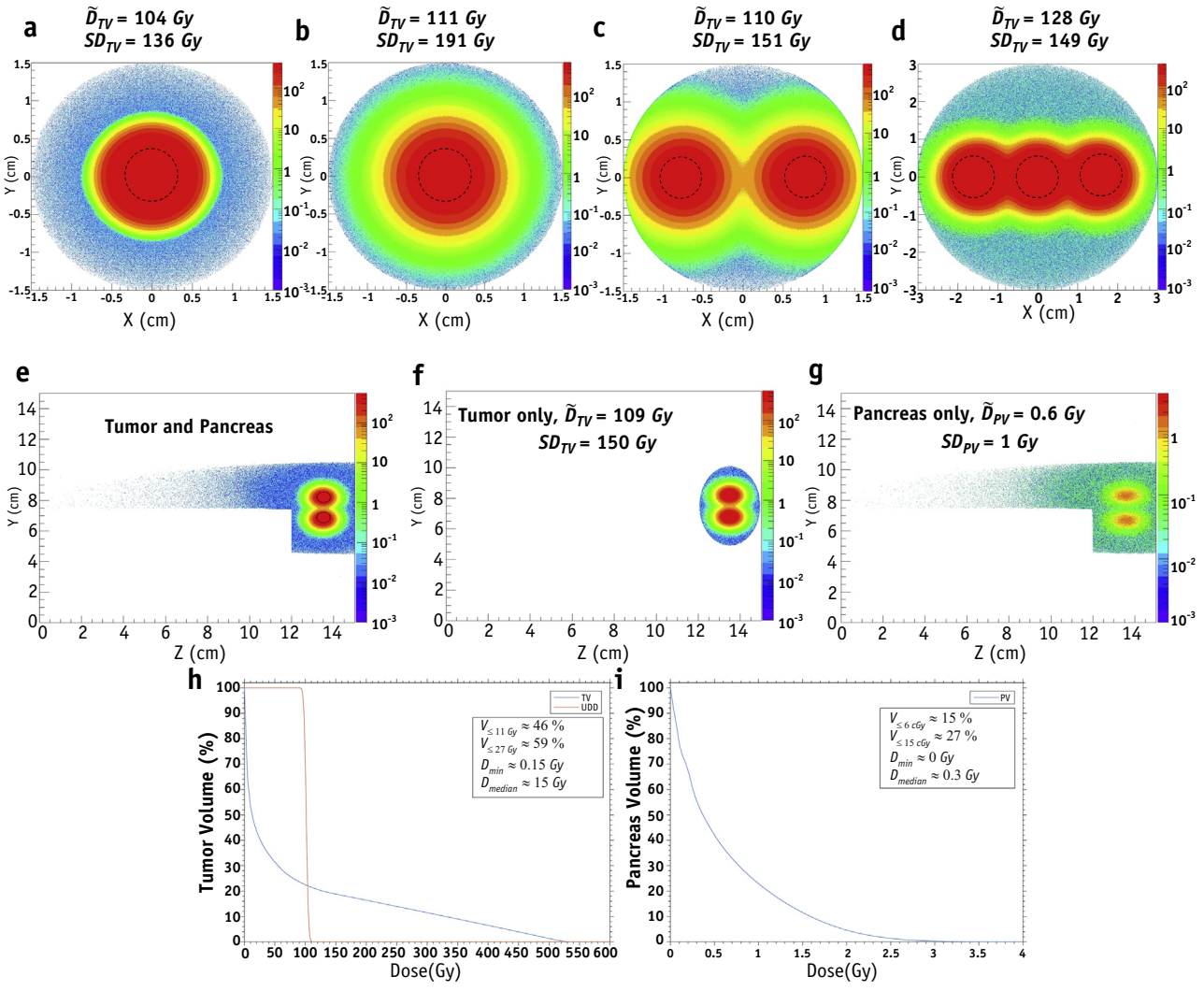

Fig. 4. Two-dimensional dose distributions for spherical tumor models and the ellipsoid tumor within the pancreas phantom. (a) A 3-cm tumor with single source and average beta energy; (b, c) 3-cm tumor with single and double sources and full beta particle energy spectrum; (d) 6-cm tumor with triple source and full beta particle energy spectrum; (e-g) 2D dose distribution of the ellipsoid tumor in the pancreas, the ellipsoid tumor only, and the pancreas phantom itself, respectively; (h, i) cumulative dose–volume histograms for the ellipsoid tumor and pancreas volumes compared with cumulative dose–volume histograms assuming a uniform dose distribution to the tumor at the mean value, ≈109 Gy. Black dotted circles indicate the edges of the treated volumes. $\tilde{D}_{TV}$ and $\tilde{D}_{PV}$ are average dose to the tumor volume (TV) and pancreas volume (PV), along with their corresponding standard deviations, SD_{TV} and SD_{PV}.

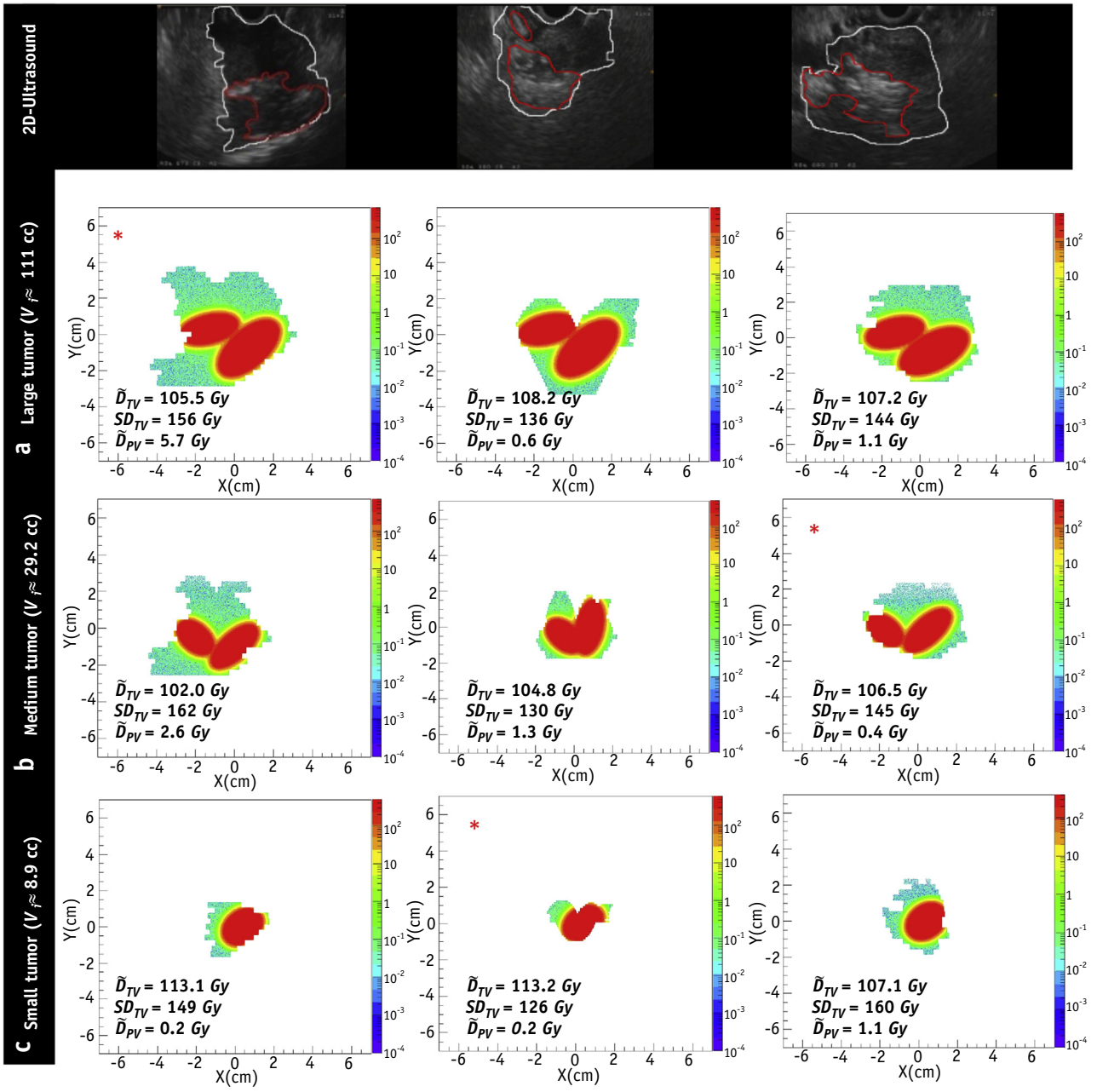

Fig. 5. Calculated 2-dimensional dose distributions for the 9 modeled irregular tumors based on individual patient ultrasound images: a) large tumor; b) medium tumor; c) small tumor. V_i denotes the initial tumor volume. $\tilde{D}_{TV}$ and $\tilde{D}_{PV}$ are the average dose to the tumor volume (TV) and to the pancreatic volume (PV), respectively, and SD_{TV} is the standard deviation in the dose to the tumor volume. Plots with a red asterisk (∗) indicate tumor models were used for simulating the dosimetry of dynamically changing tumors. (A color version of this figure is available at www.redjournal.org.)

tumor volume over the course of the treatment have an impact on dose deposited both inside the tumor and outside (ie, pancreas). For the small tumor the simulation of a static volume predicts an average dose delivered in the first 8 weeks of treatment of 113 Gy, whereas the dynamic volume simulation predicts 148 Gy. Indeed, in all 3 cases (small, medium, and large tumors) our results indicate that the assumption of a static tumor volume underpredicts the actual delivered dose, with a larger discrepancy for smaller initial tumor volumes.

The simulation results also reveal that the change in tumor volume has the greatest impact on organ dose outside the largest tumor. The average dose to the pancreas was 19 Gy, which is $\approx$16% of the tumor dose. This is mainly due to the inadequate spatial coverage of the dose delivered to the tumor. Note that if a static tumor volume is assumed, then the average dose to the pancreas drops to 5.6 Gy, which is only $\approx$5% of the tumor dose. Thus, assuming a static tumor volume underestimates the absorbed dose to the healthy parenchyma.

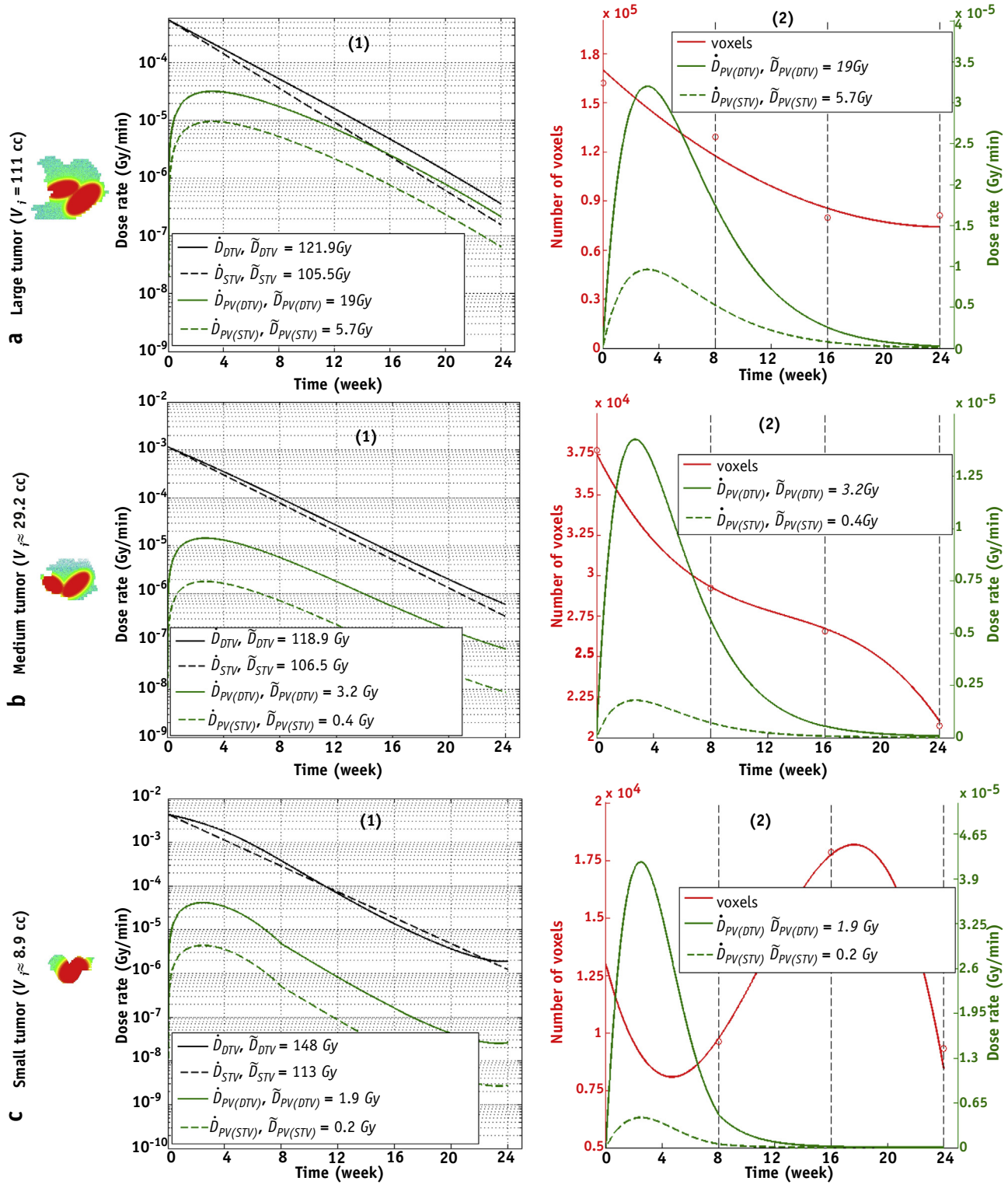

Fig. 6. Left: Dose rate ($\dot{D}$) delivered to a large (a), medium (b), and small (c) tumor with initial volumes (V_i) $\approx$ 8.9, 29.2, and 111 cm^3, and to the volume outside (healthy pancreas), as a function of treatment time. STV and DTV denote a static tumor volume and the dynamic tumor volume, respectively. Right: Corresponding number of voxels in each tumor volume as a function of treatment time (polynomial fit to measurements taken at 0, 8, 16, and 24 weeks) compared against changing dose rate. $\tilde{D}_{STV}$, $\tilde{D}_{DTV}$, $\tilde{D}_{PV(STV)}$, and $\tilde{D}_{PV(DTV)}$ are the average doses delivered to a static tumor volume, the dynamic tumor volume, the pancreas volume for static, and dynamic tumor volume, respectively.

Discussion

Dose distribution in spherical and pancreatic tumors

For the spherical tumor models, our simulation results (Fig. 4a-d) clearly show the non-uniform distribution of dose that peaks at the injection site and declines rapidly, spatially localizing tumor coverage to a radius limited by the maximum range of the beta particles (8.2 mm in water). Our results also show the strong non-uniformity in dose within the coverage area. This demonstrates the limitations of commonly used dosimetry software (eg, OLINDA) that assume a uniform dose distribution throughout a tumor. Our simulations indicate that multiple injections would be required to achieve an approximately uniform dose distribution in a 3-cm diameter tumor; 3 injections, for example, would reduce the SD by ≈20% compared with a single injection.

For the more realistic pancreatic tumor model, our simulations (Fig. 4e-g) also suggest that more than a single injection of ^{32}P will give better tumor coverage and dose uniformity in the pancreatic head, while minimizing exposure to the surrounding pancreas. The CDVHs show that ≈90% of the pancreas volume receives <1.5 Gy (Fig. 4i). For the tumor volume CDVH, Figure 4h shows that a uniform dose distribution at the mean dose value is a poor approximation of the actual distribution. This is important because it is the minimum dose to the tumor that is mostly likely to affect the tumor response to treatment: cancer cells receiving a dose below an effective dose may proliferate and lead to tumor progression or recurrence, whereas cells receiving a dose above an effective dose should receive lethal damage.

Dose distribution in irregularly shaped tumors and surrounding pancreas

For the tumor models based on clinical patient ultrasound data (Fig. 5), our simulations indicate that more source sites (injections of ^{32}P) may be needed to achieve adequate dose coverage of the tumor. The radiobiological effects of non-uniformity in tumor coverage can be quantified with the equivalent uniform dose calculation, based on the extended linear-quadratic model for a nonconstant, exponentially decreasing dose rate (4, 13, 14). This requires information on the tissue radiosensitivity and DNA repair parameters for patient-specific pancreatic tumor cell lines. Although this information was not obtained for the patients whose clinical data were used in this study, in principle it promises a personalized approach to treating advanced pancreatic cancer with ^{32}P microparticles.

For tumors larger than 10 cm^3, our results indicate that more than 1 injection is needed. The dose to the pancreas varies depending on tumor volume and the degree of irregularity in tumor shape. The worst case scenario was for a large tumor that received 105.5 Gy mean dose, but 5.7 Gy (≈5%) was delivered to the pancreas. This absorbed dose is still lower than the dose that is delivered to the pancreas from other IRT procedures. For example, a previous clinical study (15) found that IRT with an ^{131}I radiolabeled antibody for patients with peritoneal carcinomatoses could result in an absorbed dose of 2.87 to 7.75 Gy to the pancreas. It was suggested that this range of dose to the organ is unlikely to result in acute symptoms or subacute disturbance in pancreatic function. Nevertheless, the tail of the pancreas is the most critical organ component because radiation toxicity in the tail could result in diabetes. This is an important issue for external beam radiation therapy because the absorbed dose to the pancreas could be as high as ≈20 to 29 Gy (16). Our simulation results indicate that comparatively little dose is delivered to the pancreatic tail by ^{32}P microparticle treatment.

Dosimetry of dynamic tumors

For the models in which shrinkage and growth of tumors during treatment were considered, our results (Fig. 6) show that the initial tumor volume is an important determinant of the response to the time-varying dose delivered to the tumor. Assuming the tumor volume remains static throughout the treatment results in an under-prediction of the actual delivered dose, and this has the most significant impact on smaller tumors that can vary in size more dynamically than larger tumors. Although all the tumors (modeled as large, medium, or small) shrank in the first 8 weeks of treatment, in response to the peak in dose rate of delivered ^{32}P, the rapid increase in volume in the middle 8 weeks for the small tumor correlated with the rapid decay in dose rate. This tumor swelling may be a sign of edema, but no further clinical data are available to corroborate this. Interestingly, in the final 8 weeks of treatment the small tumor shrank rapidly, despite the negligible dose rate. Although this swelling followed by shrinkage may simply represent a lag in response to the radiation treatment, another possible explanation is that the tumor, compromised by the initial radiation treatment, becomes responsive to the upregulated immune system. Indeed, previous studies (17) have shown that localized irradiation of a pancreatic tumor can change the tumor microenvironment, causing inflammatory cytokines and thus increasing trafficking and retention of T lymphocytes to the tumor. It is possible that a synergistic effect may be in play: the initial high rate and localization of dose deposition within the first 8 weeks of ^{32}P treatment inflicts sufficient damage to the tumor that it eventually succumbs to the immune system's response, which is then primarily responsible for the observed treatment response—a marked decrease in tumor volume during the third 8-week period after injection of ^{32}P. The immuno-responsive mechanism could include an increased activity of lymphocytes into the tumor microenvironment, thereby enhancing tumor cell recognition and

killing through upregulation of tumor antigens and induction of positive immunomodulatory pathways (17-20).

A similar effect has been observed in the case of external beam radiation therapy and selective internal radiation therapy, whereby delivery of a high and localized dose has led to systemic responses at distant sites, a phenomenon known as the abscopal effect, which has been attributed to the induction and enriching of the immune response (21-26).

However, because the patients were also treated with gemcitabine, a chemotherapeutic with radiosensitizing properties (27), the observed tumor shrinkage in the final weeks of treatment, when activity was negligible, may be attributable to the effects of this drug (28, 29). Further clinical studies are needed to confirm this.

Conclusion

Our results have determined that for a clinically prescribed activity in the range 5 to 60 MBq, ^{32}P microparticles deliver a $\approx$100- to 120-Gy mean dose to a pancreatic tumor volume. Our results also suggest that for clinically relevant tumor shapes, multiple injections may be required to overcome the non-uniform activity distribution. We found that for 2 injections, the organ dose remains limited to 5% to 6% of the tumor dose in the worst case scenario studied. Our study also highlights the limitation of assuming a uniform mean dose distribution. We found significant deviations from the mean dose value, including a nonnegligible number of cold voxels that potentially present a risk of tumor recurrence or proliferation. Additionally, this study demonstrates the importance of considering the dynamic change in tumor volume in internal radionuclide therapy dosimetry. Dosimetry of both the tumor and adjacent critical organs is affected by the dynamic change of the tumor mass during treatment, and this effect is generally more pronounced for small tumors that initially shrink at a rate faster than the radioisotope decay rate. Our simulation and modeling results, based on patient-specific data, demonstrate the efficacy of ^{32}P microparticles in treating advanced pancreatic cancer and the possibility of designing personalized treatment strategies.

References

1. Delpassand ES, Samarghandi A, Zamanian S, et al. Peptide receptor radionuclide therapy with 177Lu-DOTATATE for patients with somatostatin receptor-expressing neuroendocrine tumors. *Pancreas* 2014;43:518-525.
2. Sahar AK, Cao A, Coa Q. Radioembolization of yttrium-90 microspheres for clinical treatment of hepatic malignancy. *J Nucl Med Radiat Ther* 2014;5:187.
3. Taneja SS. Re: Alpha emitter radium-223 and survival in metastatic prostate cancer. *J Urol* 2014;191:657.
4. Kalogianni E, Flux G, Malaroda A. The use of BED and EUD concepts in heterogeneous radioactivity distributions on a multicellular scale for targeted radionuclide therapy. *Cancer Biother Radiopharm* 2007;22:43-150.
5. Goddu SM, Howell RW, Rao DV. Generalized approach to absorbed dose calculations for dynamic tumor and organ masses. *J Nucl Med* 1995;36:1923-1927.
6. Kost S, Dewaraja Y, Abramson R, et al. VIDA: A voxel-based dosimetry method for targeted radionuclide therapy using Geant4. *Cancer Biother Radiopharm* 2015;30:16-26.
7. Jan S, Santin G, Strul D, et al. GATE: A simulation toolkit for PET and SPECT. *Phys Med Biol* 2004;2004:4543.
8. Agostinelli S, Allison J, Amako KA, et al. Geant4—a simulation toolkit. *Nucl Instr Methods Phys Res A* 2003;506:250-303.
9. Ouellet C, Balraj S. Nuclear data sheets for A = 32. *Nuclear Data Sheets* 2011;112:2199-2355.
10. Chauvie S, Guatelli S, Ivanchenko V, et al. Geant4 low energy electromagnetic physics. *IEEE Nucl Sci Conf R* 2004;3:1881-1885.
11. Cristy M, Eckerman KF. Specific Absorbed Fractions of Energy at Various Ages from Internal Photon Sources. Report ORNL/TM 8381/v1-v7. Oak Ridge, TN: Oak Ridge National Laboratory; 1987.
12. Stabin MG. Fundamentals of Nuclear Medicine Dosimetry. New York: Springer; 2008.
13. Dale RG. Dose-rate effects in targeted radiotherapy. *Phys Med Biol* 1996;41:1871-1884.
14. Dale R, Carabe-Fernandez A. The radiobiology of conventional radiotherapy and its application to radionuclide therapy. *Cancer Biother Radiopharm* 2005;20:47-51.
15. Larson SM, Carrasquillo JA, Colcher DC, et al. Estimates of radiation absorbed dose for intraperitoneally administered iodine-131 radiolabeled B72.3 monoclonal antibody in patients with peritoneal carcinomatoses. *J Nucl Med* 1991;32:1661-1667.
16. de Vathaire F, El-Fayech C, Ben Ayed FF, et al. Radiation dose to the pancreas and risk of diabetes mellitus in childhood cancer survivors: A retrospective cohort study. *Lancet Oncol* 2012;13:1002-1010.
17. Shiao SL, Coussens LM. The tumor-immune microenvironment and response to radiation therapy. *J Mammary Gland Biol Neoplasia* 2010;15:411-421.
18. Yoshimura M, Itasaka S, Harada H, et al. Microenvironment and radiation therapy. *Biomed Res Int* 2013;2013:6858308.
19. Vatner R, Cooper B, Vanpouille-Box C, et al. Combinations of immunotherapy and radiation in cancer therapy. *Front Oncol* 2014;4:325.
20. Park B, Yee C, Lee K. The effect of radiation on the immune response to cancers. *Int J Mol Sci* 2014;15:927-943.
21. Aoyama H, Shirato H, Kakuto Y, et al. Pathologically-proven intracranial germinoma treated with radiation therapy. *Radiother Oncol* 1998;47:201-205.
22. Ross GM. Induction of cell death by radiotherapy. *Endocr Relat Cancer* 1999;6:41-44.
23. Levy A, Chargari C, Marabelle A, et al. Can immunostimulatory agents enhance the abscopal effect of radiotherapy? *Eur J Cancer* 2016;62:36-45.
24. Formenti S, Demaria S. Systemic effects of local radiotherapy. *Lancet Oncol* 2009;10:718-726.
25. Formenti S, Demaria S. Radiation therapy to convert the tumor into an in situ vaccine. *Int J Radiat Oncol Biol Phys* 2012;84:879-880.
26. Ghodadra A, Bhatt S, Camacho J, et al. Abscopal effects and yttrium-90 radioembolization. *Cardiovasc Intervent Radiol* 2015;39:1076-1080.
27. Pauwels B. Combined modality therapy of gemcitabine and radiation. *Oncologist* 2005;10:34-51.
28. Oettle H, Post S, Neuhaus P, et al. Adjuvant chemotherapy with gemcitabine vs observation in patients undergoing curative-intent resection of pancreatic cancer: A randomized controlled trial. *JAMA* 2007;297:267-277.
29. Plate JM, Plate AE, Shott S, et al. Effect of gemcitabine on immune cells in subjects with adenocarcinoma of the pancreas. *Cancer Immunol Immunother* 2005;54:915-925.